

Modelling of functional profiles and explainable shape shifts detection: An approach combining the notion of the Fréchet mean with the shape invariant model

G. I. Papayiannis^{*a,d}, S. Psarakis^{b,c}, and A. N. Yannacopoulos^{b,d}

^aSection of Mathematics, Department of Naval Sciences, Hellenic Naval Academy, Piraeus, GR 18539

^bDepartment of Statistics, Athens University of Economics & Business, Athens, GR 10434

^cLaboratory of Statistical Methodology, Athens University of Economics and Business, Athens, GR 10434

^dStochastic Modelling and Applications Laboratory, Athens University of Economics & Business, Athens, GR 10434

Abstract

A modelling framework suitable for detecting shape shifts in functional profiles combining the notion of Fréchet mean and the concept of deformation models is developed and proposed. The generalized mean sense offered by the Fréchet mean notion is employed to capture the typical pattern of the profiles under study, while the concept of deformation models, and in particular of the shape invariant model, allows for interpretable parameterizations of profile's deviations from the typical shape. EWMA-type control charts compatible with the functional nature of data and the employed deformation model are built and proposed, exploiting certain shape characteristics of the profiles under study with respect to the generalised mean sense, allowing for the identification of potential shifts concerning the shape and/or the deformation process. Potential shifts in the shape deformation process, are further distinguished to significant shifts with respect to amplitude and/or the phase of the profile under study. The proposed modelling and shift detection framework is implemented to a real world case study, where daily concentration profiles concerning air pollutants from an area in the city of Athens are modelled, while profiles indicating hazardous concentration levels are successfully identified in most of the cases.

Keywords:

deformation models; EWMA control charts; Fréchet mean; functional profiles; shape invariant model; shift detection;

1 Introduction

The task of efficient modelling and the accurate identification of potential shifts for functional profiles has attracted the interest of the statistical community the later years. Such kind of data structures are met more and more in practice in many fields, for instance, in medicine and medical imaging, in electricity management, in water distribution networks, in environmental sciences, etc. The development of more elaborate and complex monitoring schemes is required for the statistical treatment of dynamical and functional data structures in order to reveal and recover important information concerning the special features of the process under study. The resulting functional data (and their increased complexity) is an issue that at a first stage can be handled either by the application of non-linear models or by non-parametric or semi-parametric approaches (e.g. kernel-based estimators, wavelets, etc.). However, as far as statistical control

*Corresponding author: [gpapagiannis@aueb.gr](mailto:gpagagiannis@aueb.gr) g.papagiannis@hna.gr

is concerned, for these functional models the classical control tools may not be appropriate; partly because of their functional nature and partly because the output of such models may not be appropriately accommodated in a vector space framework. This fact imposes the need for development of new monitoring mechanisms compatible with the functional data setting. Particularly, in the field of functional profiles monitoring, several approaches have been proposed lately, and to mention just a few, non-parametric regression or wavelets approaches Chicken et al. (2009); Qiu et al. (2010); McGinnity et al. (2015), interpolation schemes Moguerza et al. (2007); Fassò et al. (2016), PCA and functional PCA-based methods Shiau et al. (2009); Yu et al. (2012); Paynabar et al. (2016), functional regression Centofanti et al. (2021), approaches exploiting the intrinsic geometry of appropriate statistical manifolds or relying on the notion of statistical depth Harris et al. (2020); Zhao and Del Castillo (2021) and others. The majority of the aforementioned approaches attempt through modifications in the modelling procedure, but still relying on the current setting of process control theory and practice, to extent the current monitoring tools to better treat the new modeling setup, accommodating certain of the salient features of the data in question (such as functional dependence etc).

A crucial issue in studying functional profiles from the monitoring perspective, concerns the actual definition of the typical or the so called *in control* (IC) behaviour. Standard approaches assume that the under study data can be represented as points of a finite dimensional Euclidean space (e.g. of \mathbb{R}^d) of suitable dimensionality related to the number of features under consideration, possibly carrying a correlation structure or displaying variability which is modelled essentially under the assumption of a probability law similar or sufficiently close to a Gaussian one. On the context of functional data, the above setting is not appropriate for a number of reasons. To name just a few:

- (a) The finite dimensionality assumption is no longer valid as the data in question are infinite dimensional, e.g. curves, shapes, surfaces.
- (b) The dependence structure displayed by data may not be sufficiently modelled within the normality assumption since more complex type of dependencies may be displayed which cannot be approximated by the Gaussian model.
- (c) The observed data may no longer be understood as elements of a vector space but as elements of a space with nonlinear or convex structure (e.g. elements of a general metric space like covariance matrices, curves of particular form, etc).

Recently, Cano et al. (2015) initiated the development of a more appropriate framework for dealing with functional data, employing tools from the statistical shape theory (see e.g. Dryden and Mardia (2016); Small (2012)). In the current work, we emphasize on the appropriate definition and estimation of the typical behaviour of the objects under study, through a more general notion of mean, applicable for metric space valued data, the Fréchet mean, combined with the framework of deformation models. The approach we propose and develop is quite general and can be applied to any functional object (e.g. curves, surfaces, etc.), however we restrict ourselves to the case of profiles represented by curves in order to properly motivate the proposed methodology. Attempting to provide a more concrete framework, we focus on the case of the shape invariant model (SIM), a functional modelling approach which is widely applicable to various contexts. Nevertheless, the discussed framework is extendable to any other deformation model choice beyond SIM.

The paper is organized in the following way. In Section 2 some important preliminaries concerning the notion of the Fréchet mean and the framework of deformation models are presented accompanied by a brief literature overview. In Section 3, our modelling setup combining the notion of the Fréchet mean and the shape invariant model is presented accompanied by appropriate numerical approximation schemes for estimating the mean pattern (i.e. the reference profile or the Fréchet mean) and, registering a sampled profile to the reference one according to the

shape invariant deformation model. Next, in Section 4, a two-step shape shift detection scheme is proposed, by appropriately extending the exponentially weighted moving average (EWMA) scheme framework to the case of non-vector spaces. In particular, employing the adopted deformation modelling approach and the notion of Fréchet mean, the developed scheme allows for the detection of potential shifts in the underlying shape of the profile under study, at the first step, and for detecting potential shifts in the deformation process of the profile compared to the typical pattern, at the second step. The latter step, allows for further investigation of the shift (if occurred) and categorizing it in terms of shifts in certain characteristics related to amplitude or phase. Then, the proposed approach is implemented to a real world example where, ambient air quality profiles in an area of the city of Athens are modelled, and applying the proposed shift detection method, out of control behaviours are successfully identified in most of the cases.

2 Literature Overview & Preliminaries

Here we briefly introduce and discuss the notion of Fréchet mean and the framework of deformation models which are the basic concepts on which our work on functional profiles modelling and monitoring relies on.

2.1 Fréchet mean: a generalized version of the mean

Functional objects like profiles, curves, surfaces, etc. are not objects that necessarily belong to a vector space. For instance, if a profile is subject to some distortion, it is not necessary that this output can be represented under the application of linear operations on the possible profiles of the space under study. In fact, the representation of the distorted profile is not guaranteed by a vector space, even if we know that the distortion is of linear type with respect to the amplitude and phase, since the aggregate distortion would be nonlinear with respect to the profile itself (see for example the effect of the shape invariant model which is examined in this work). As such, the typical notion of mean is not applicable in this case since there is not the typical vector space setting. This motivates the need for a notion of the mean that does not rely on linearity. Such a generalized notion of the mean which is widely applicable is offered by the Fréchet mean Fréchet (1948); Zemel and Panaretos (2019), which for a sample of random elements $\{x_1, \dots, x_n\} \subset \mathcal{M}$ is defined as

$$(1) \quad x_F := \arg \min_{z \in \mathcal{M}} \Psi(z)$$

where $\Psi(z) = \sum_{j=1}^n w_j d^2(z, x_j)$ is the generalized Fréchet function of the sample, d is a suitable metric for the space \mathcal{M} and $\{w_1, \dots, w_n\}$ is a suitable set of weights for the data (the case $w_i = 1/n$ corresponds to the standard definition of the Fréchet mean). The minimum value of Ψ (achieved at x_F) corresponds to the variance of the sample. The Fréchet mean is a variational concept that can be obtained using techniques from the calculus of variations and optimization (see e.g. Kravvaritis and Yannacopoulos (2020)) and its theoretical properties are well documented (see e.g. Le and Kume (2000); Afsari (2011); Arnaudon et al. (2013); Petersen et al. (2019)). It has been recently used by the statistics community as an important tool in the study of data which cannot be conveniently described as elements of vector spaces (see e.g. Dubey and Müller (2019), Izem et al. (2007), Jung et al. (2012), etc). In the monitoring framework presented in this work, the Fréchet mean is employed to capture the typical pattern or mean behaviour of an IC sample of functional profiles. However, the performance of this approach significantly depends on the suitability of the deformation model that is chosen to model the variations around the typical pattern (in the case that a semi-parametric approach is adopted) and of course the metric sense under which the operations are derived.

2.2 The framework of deformation models

A very natural setting for the study of functional profiles is that of deformation models. Deformation models produce metric space valued random elements which belong to some set $\mathcal{M} = \{f \circ T : T \in V\}$ where f is a deterministic function (often to be specified) characterizing the typical (average) shape, and $T(\cdot) = T(\cdot, \omega)$ is a random deformation typically chosen from a vector space V so that the composition $f \circ T(\cdot, \omega)$ generates a random element from \mathcal{M} , satisfying certain qualitative features. Hence, each random element is parameterized in terms of the realization of $T \in V$. For example, f can be the curve modeling the distribution of some pollutant over the day, accounting for patterns like the mean variability of traffic or the mean variability of temperature, while T accounts for specific features that may randomly happen on a particular day and may not repeat. We emphasize that in many case of interest \mathcal{M} is not endowed with a linear structure (e.g. in the case of s -shaped curves) but is rather a subset of a more general metric space. For instance, consider curves of a specific shape as those appear in medicine (e.g. intra-day blood pressure curves) or those describing the intra-day demand of electric energy in a city or daily consumption patterns over a water distribution network. Such objects do not necessarily belong to a vector space, since summing two sampled objects does not necessarily leads to an object of the underlying space. This type of statistical modelling has found several applications in practice so far, e.g., in image and signal processing Bigot et al. (2009, 2011), in analysing point processes Panaretos et al. (2016), in medicine Papayiannis et al. (2018), in electric energy prediction Kampelis et al. (2020), etc. Restricting attention to the case where $f : I \rightarrow \mathbb{R}$ is a function from some interval of I ($I = [0, 1]$ without loss of generality) is a suitable choice for the study of nonlinear profiles. A more generic form of a deformation model has been studied in Panaretos et al. (2016), modeling separately amplitude and phase deformation characteristics. Under the perspective of the general *amplitude-phase* deformation model, the shape relation between two curves f and g is expressed as

$$(2) \quad f(t) = A(g(\Phi^{-1}(t))) + \epsilon(t)$$

where $\Phi : I \rightarrow I$ for $I \subset \mathbb{R}$ represents the *phase deformation process* (its inverse Φ^{-1} is often referred to as the *time-warping function* according to the terminology of Wang et al. (1997)) and $A : L^2(I) \rightarrow L^2(I)$ ¹ represents the *amplitude deformation process*, while $\epsilon(t)$ denotes the relevant error term, i.e. the aspects of curve f that cannot be efficiently captured through a deformation of g under the particular shape deformation modeling approach. Parametric forms of Φ and A are conceivable and practical and hence often used in practice (see e.g. Kneip and Engel (1995); Wang et al. (1997); Gervini and Gasser (2004)). Considering affine parametric forms for both phase and amplitude deformation process, i.e. $A(z) = \alpha z + b$ and $\Phi(s) = \kappa s + \zeta$, reduces the amplitude-phase deformation model to the well celebrated shape invariant model on which the presented approach relies on.

3 A Functional Modelling Approach Combining the Shape Invariant Model Framework and the Notion of the Fréchet Mean

In this section we provide a modelling framework for functional profiles which allows the parameterization of an individual's profile deviance with respect to the typical pattern. In particular, we focus on the shape invariant deformation model which consider linear deformations with respect to the amplitude and phase characteristics separately (but still nonlinear with respect to the reference shape). Relying on this deformation model, the Fréchet mean of a set of profiles is approximated by appropriately formulating the Fréchet variance determination problem and proposing a numerical approximation scheme for this purpose. Moreover, we consider the

¹ $L^2(I)$: the Lebesgue space of square integrable functions with domain I

registration problem of a sampled profile to the reference shape (Fréchet mean) providing the related well posedness results.

3.1 A brief presentation of the shape invariant deformation model

The shape invariant model has been repeatedly discussed and appreciated in the functional modelling literature (see e.g. Kneip and Engel (1995); Gervini and Gasser (2004); Beath (2007); Bigot et al. (2013)) due to its applicability in various different contexts and the interpretability of its deformation parameters. Under this setting, an object f_j is modeled as a distortion of the typical profile f_0 through the relation

$$(3) \quad f_j(t) = \beta_j + \alpha_j f_0\left(\frac{t - \zeta_j}{\kappa_j}\right) + \epsilon_j(t), \quad t \in I$$

which can be realized as a special case of the general amplitude-phase deformation model (see e.g. Panaretos et al. (2016)) considering $A_j(z) = \alpha_j z + \beta_j$ and $\Phi_j(s) = \kappa_j s + \zeta_j$ with (α_j, β_j) denoting the deformation parameters related to the scale and location of the amplitude deformation process, while (κ_j, ζ_j) denoting the parameters affecting the scale and location of the phase deformation process (please see Figure 1 for an illustration of the deformation model's characteristics). In this perspective, the space of profiles \mathcal{M} is identified by the following subset of L^2

$$(4) \quad \mathcal{M} := \left\{ f \in L^2 : \exists (\alpha, \beta, \kappa, \zeta)' \in \Theta \subset \mathbb{R}^4 \text{ where } f(t) = \beta + \alpha f_0\left(\frac{t - \zeta}{\kappa}\right), \quad t \in I \right\}$$

with the set Θ including the feasible values for the deformation parameters, leading to a metric space setting which does not carry the linear structure of a vector space.

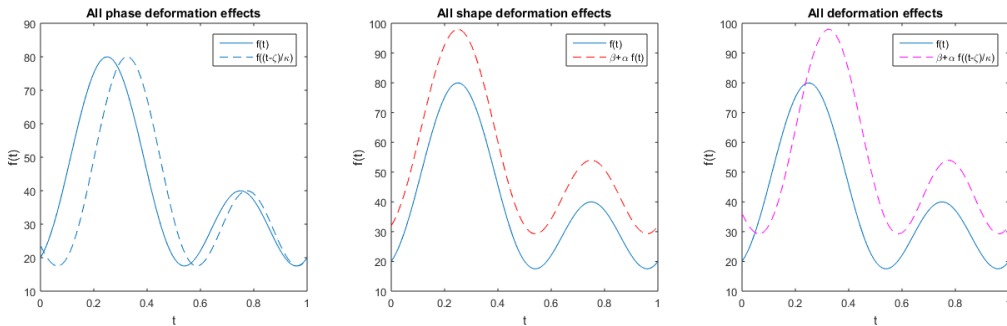


Figure 1: Shape-invariant model parameterization effects for phase deformations (left), shape deformations (center) and both types of deformations (right).

3.2 Determination of the typical profile under the shape invariant model

Let us now assume that there is a training set of profiles $\mathcal{F} := \{f_1, f_2, \dots, f_n\}$, and that each profile f_j can be sufficiently modeled as a deformation of the (unknown yet) mean profile f_0 , as represented in (3), with deformation parameters $\theta_j = (\alpha_j, \beta, \kappa_j, \zeta_j)'$. Amplitude distortion of f_j comparing to the reference (Fréchet mean) profile f_0 is captured by the deformation function $A(t; \gamma_j) = \beta_j + \alpha_j f_0(t)$ with $\gamma_j := (\beta_j, \alpha_j)'$ denoting the amplitude deformation parameters, while phase distortions are captured by the function $\Phi(t; \xi_j) = \zeta_j + \kappa_j t$ with $\xi_j = (\zeta_j, \kappa_j)'$ denoting the relevant phase deformation parameters. These parameterized effects cannot be specified unless the Fréchet mean is estimated. Following the current modeling approach, a semi-parametric expression of the mean is obtained through averaging. Using the model (3), one can obtain a motivation for the definition of Fréchet mean using the functional data f_j . In

particular, one may express

$$(5) \quad f_0(t) = \hat{f}_{0,j}(t; \theta_j) + \eta_j(t) = \alpha_j^{-1} (f_j(\kappa_j t + \zeta_j) - \beta_j) + \eta_j(t)$$

where $\eta_j(\cdot)$ denotes the distorted error process related to the estimation error relying on the observation from f_j . The mean profile f_0 must be chosen in such a manner that satisfies the barycenter property, i.e. being simultaneously so close and so far from all the profiles contained in the set \mathcal{F} . A standard requirement that has to be met is that the average of the residuals η_j among all elements, for each time instant $t \in I$, must be zero, i.e. $\frac{1}{n} \sum_{j=1}^n \eta_j(t) = 0$. As a result, by properly averaging every possible model of f_0 as a deformation of each $f_j \in \mathcal{F}$, we obtain the following semi-parametric expression

$$(6) \quad \hat{f}_0(t; \boldsymbol{\theta}) = \frac{1}{n} \sum_{j=1}^n \hat{f}_{0,j}(t; \theta_j) = \frac{1}{n} \sum_{j=1}^n \alpha_j^{-1} (f_j(\kappa_j t + \zeta_j) - \beta_j)$$

where $\boldsymbol{\theta} = (\boldsymbol{\alpha}', \boldsymbol{\beta}', \boldsymbol{\kappa}', \boldsymbol{\zeta}')'$ with $\boldsymbol{\alpha} = (\alpha_1, \dots, \alpha_n)'$, $\boldsymbol{\beta} = (\beta_1, \dots, \beta_n)'$, $\boldsymbol{\kappa} = (\kappa_1, \dots, \kappa_n)'$ and $\boldsymbol{\zeta} = (\zeta_1, \dots, \zeta_n)'$. Clearly, what is represented in (5) is not the pure Fréchet mean, but rather its best approximation under the shape invariant model. The optimality criterion which is employed for the selection of $\boldsymbol{\theta}$, depends on the metric sense d_M under which we wish to derive the mean element. Recalling the Fréchet function defined in (1), the optimal $\boldsymbol{\theta}_* \in \Theta$, where Θ denotes the feasible set of the deformation parameters, is obtained as the solution to the minimization problem

$$(7) \quad \min_{\boldsymbol{\theta} \in \Theta} V(\boldsymbol{\theta}) := \min_{\boldsymbol{\theta} \in \Theta} \frac{1}{n} \sum_{j=1}^n d_M^2(\hat{f}_0(\boldsymbol{\theta}), f_j)$$

leading to the determination of the Fréchet mean under the current deformation family of models. In general, the required centrality properties for the amplitude and phase deformation functions are

- $A_1 \circ A_2 \circ \dots \circ A_n = Id$
- $\Phi_1 \circ \Phi_2 \circ \dots \circ \Phi_n = Id$.

Specifying the conditions for the case of the shape invariant model, are equivalently stated by the set of constraints for the related deformation parameters

$$(8) \quad \prod_{j=1}^n \alpha_j = 1, \quad \sum_{j=1}^n \beta_j = 0, \quad \prod_{j=1}^n \kappa_j = 1, \quad \sum_{j=1}^n \zeta_j = 0$$

with α_j, κ_j being strictly positive and upper bounded by some $\alpha_{\max}, \kappa_{\max}$, while β_j and ζ_j are constrained to some appropriate intervals $[\beta_{\min}, \beta_{\max}]$ and $[\zeta_{\min}, \zeta_{\max}]$, respectively (for all $j = 1, 2, \dots, n$). These properties ensure that the total deformation effect sums up to zero, and that the derived minimizer from (7) represents the optimal reference profile since, all elements in the training set are aligned with respect to this profile, either in terms of amplitude or phase distortions. To make more clear this conditions, let us consider for instance the simple case of two profiles. Under the aforementioned centrality conditions we require the aggregate amplitude deformation effect to satisfy

$$(A_1 \circ A_2)(g) = g \iff \beta_1 + \beta_2 + \alpha_1 \alpha_2 g = g, \quad \forall g \in L^2$$

resulting to $\beta_1 + \beta_2 = 0$ and $\alpha_1\alpha_2 = 1$, while concerning the aggregate phase deformation effect it is required that

$$(\Phi_1 \circ \Phi_2)(t) = t \iff \zeta_1 + \zeta_2 + \kappa_1\kappa_2 t = t, \quad \forall t \in I$$

resulting to $\zeta_1 + \zeta_2 = 0$ and $\kappa_1\kappa_2 = 1$. Then, the obtained mean element provides a comparison pattern with respect to which, all individual elements in the training set are aligned to in terms of both phase and amplitude.

Remark 3.1. Note that a potential minimizer $\boldsymbol{\theta}_*$ of (7) contains the optimal deformation parameters concerning the approximation of the Fréchet mean of the set \mathcal{F} under the SIM approach. For a specific profile $f_j \in \mathcal{F}$ the related deformation parameters $\theta_{*,j}$ contained in the vector $\boldsymbol{\theta}_*$ does not necessarily coincide with the parameter choices that best represent the current profile as a SIM deformation with respect to the mean shape. This happens since optimal solution of (7) is subject to the set of constraints stated in (8) which are much more restrictive than the ones that are required for registering some specific f_j to the mean shape (this matter is discussed separately in the following sections). Clearly, $\boldsymbol{\theta}_*$ is the choice of parameters indicating the optimal position (or tuning) of the semi-parametric mean shape model stated in (6) with respect to all elements in the set \mathcal{F} . Clearly, this is not necessarily the same with collecting the optimal deformations of each $f_j \in \mathcal{F}$ with respect to the (estimated) mean shape $\hat{f}_0(\boldsymbol{\theta})$.

Let us consider the problem of estimating the mean profile (typical shape) under the SIM framework and employing the L_2 metric sense (i.e. $d_M(f, g) = \|f - g\|_2$ for any $f, g \in \mathcal{M}$). Then, the resulting Fréchet function minimization problem is characterized by the objective function

$$(9) \quad V(\boldsymbol{\theta}) := \frac{1}{n} \sum_{j=1}^n \langle f_j - \hat{f}_0(\boldsymbol{\theta}), f_j - \hat{f}_0(\boldsymbol{\theta}) \rangle$$

where $\langle f, g \rangle := \int_I f(s)g(s)ds$ denotes the inner-product in the $L^2(I)$ for any $f, g \in L^2(I)$ and $\hat{f}_0(\boldsymbol{\theta})$ as stated in (6). Following the discussion in the previous section, we are interested in the problem of minimizing (9) on the set Θ , denoting the feasible set for $\boldsymbol{\theta}$ satisfying all the constraints stated in (8). In order to guarantee the uniqueness of the solution (existence is guaranteed by the continuity with respect to $\boldsymbol{\theta}$), appropriate Tikhonov-type regularizations are necessary. For this reason, the quadratic regularization term $R_\rho(\boldsymbol{\theta}) = \frac{1}{2\rho} \|\boldsymbol{\theta}\|_2^2$ is introduced, driven by the sensitivity parameter $\rho > 0$. This regularization transforms, for a certain value of ρ and below, the problem to a strictly convex one. Besides the convexity-correction of the problem, the regularization term enhances the stability of the problem, not allowing to each deformation parameter exceeding a certain threshold value, which in combination with the constraints provided by the set Θ , reduces the effect of potential extreme profiles in \mathcal{F} to the estimation of the mean, robustifying the estimation procedure. Modifying the problem in this way, when more than one minimizers exist, we introduce a selection criterion among the potential solutions, placing a preference order that promotes the ones that cause less dramatic deformations with respect to the original profiles in \mathcal{F} . The related result follows (for the relevant proof please see Appendix A.1).

Proposition 3.2. *There exists $\rho_0 > 0$ for which the regularized Fréchet variance determination problem*

$$(10) \quad \min_{\boldsymbol{\theta} \in \Theta} \left\{ V(\boldsymbol{\theta}) + \frac{1}{2\rho} \|\boldsymbol{\theta}\|_2^2 \right\}$$

admits unique solution for any $\rho \in (0, \rho_0]$.

3.3 A numerical spitting approach for the approximation of the mean profile

Next, we consider the development of a numerical approximation scheme for estimating the mean profile under SIM framework, i.e. approximating the optimal solution of problem (7). First, we distinguish the dependence of function V to the amplitude deformation parameters $\gamma = (\alpha', \beta)'$ and to the phase deformation parameters $\xi = (\kappa', \zeta)'$. Splitting the parameters into two distinct groups is a key step towards the development of an efficient numerical approximation scheme. Ignoring at first the centrality constraints (8) and under appropriate transformations of the parameters contained in γ^2 , the function V depends quadratically on the amplitude deformation parameters, while as far as the parameter vector ξ is concerned, the dependence is non-quadratic and importantly non-convex (at least in general cases). Treating directly the problem with respect to all the parameters, results to a non-convex and computationally expensive minimization problem which is difficult to treat. Alternatively, we propose an iterative parameter-splitting minimization scheme, which treats the problem in two separate stages and takes advantage over the quadratic dependence of V with respect to γ and by convexly approximating the solution with respect to ξ . Tikhonov-type regularizations are considered to both parts of the problem (for different reasons) and through successive projections of the obtained solutions to the constrained sets an optimal solution is reached.

Let us decompose the parameter space Θ to two components Θ_Λ and Θ_Π (satisfying $\Theta = \Theta_\Lambda \times \Theta_\Pi$) as follows

$$(11) \quad \Theta_\Lambda = \left\{ \gamma = (\bar{\alpha}', \bar{\beta}')' \in \mathbb{R}^{2n} : \prod_{j=1}^n \bar{\alpha}_j = 1, \sum_{j=1}^n \frac{\bar{\beta}_j}{\bar{\alpha}_j} = 0, \bar{\alpha}_j > 0, \forall j \right\}$$

$$(12) \quad \Theta_\Pi = \left\{ \xi = (\kappa', \zeta')' \in \mathbb{R}^{2n} : \prod_{j=1}^n \kappa_j = 1, \sum_{j=1}^n \zeta_j = 0, \zeta_j \in [\zeta_{\min}, \zeta_{\max}], \forall j \right\}.$$

To clarify the separate dependence of V to the amplitude deformation parameters γ and to the phase deformation parameters ξ , we denote equivalently from now on the respective Fréchet function as $V(\gamma, \xi)$. Regularization terms of the form suggested in Proposition (3.2) are introduced to the problem separately for γ and ξ . Fixing a choice ξ , the (unconstrained) minimization problem with respect to γ can be solved in closed form, while a regularization term is required for stabilizing the estimation procedure. Then, the solution is projected to its constrained set Θ_Λ . Subsequently, fixing the obtained γ , the (unconstrained) minimization problem with respect to ξ is solved, introducing a regularization term that will guarantee the convexity of the objective function. The obtained solution ξ is projected to its constraint set Θ_Π and the above steps are repeated till convergence. The scheme in algorithmic formulation is described below.

Algorithm 3.3 (Iterative splitting-projection scheme for Fréchet mean approximation).

0. Set $k = 1$, $\gamma^{(0)} = (1, 1, \dots, 1, 0, 0, \dots, 0)'$, $\xi^{(0)} = (1, 1, \dots, 1, 0, 0, \dots, 0)'$ and specify a tolerance level ($\epsilon > 0$).

1. Solve the amplitude-unconstrained optimization problem

$$(13) \quad \hat{\gamma} = \arg \min_{\gamma \in \mathbb{R}^{2n}} \left\{ V(\gamma, \xi^{(k-1)}) + \frac{1}{2\rho} (\|\gamma\|_2^2) + \|\xi^{(k-1)}\|_2^2 \right\}, \quad \rho > 0$$

and then compute the projection $\gamma^{(k)} = Proj_{\Theta_\Lambda}(\hat{\gamma})$

²considering $\gamma := (\bar{\alpha}', \bar{\beta}')'$ with $\bar{\alpha}_j := 1/\alpha_j$ and $\bar{\beta}_j := \beta_j \bar{\alpha}_j$ for $j = 1, 2, \dots, n$

2. Solve the phase-unconstrained optimization problem

$$(14) \quad \hat{\boldsymbol{\xi}} = \arg \min_{\boldsymbol{\xi} \in \mathbb{R}^{2n}} \left\{ V(\boldsymbol{\gamma}^{(k)}, \boldsymbol{\xi}) + \frac{1}{2\rho} \left(\|\boldsymbol{\xi}\|_2^2 + \|\boldsymbol{\gamma}^{(k)}\|_2^2 \right) \right\}, \quad \rho > 0$$

and then compute the projection $\boldsymbol{\xi}^{(k)} = \text{Proj}_{\Theta_{\Pi}}(\hat{\boldsymbol{\xi}})$

3. If $\|\boldsymbol{\gamma}^{(k)} - \boldsymbol{\gamma}^{(k-1)}\| < \epsilon$ and $\|\boldsymbol{\xi}^{(k)} - \boldsymbol{\xi}^{(k-1)}\| < \epsilon$ stop and set $(\boldsymbol{\gamma}_*, \boldsymbol{\xi}_*) = (\boldsymbol{\gamma}^{(k)}, \boldsymbol{\xi}^{(k)})$. Else set $k = k + 1$ and return to *Step 1*.

The aforementioned alternative projections-splitting scheme converges to a unique solution from standard arguments from the theory of alternating projections. The result is stated in the following proposition (for more details please see Appendix A.2).

Proposition 3.4. *The following hold:*

- a. Given $\boldsymbol{\gamma}^{(0)} \in \Theta_{\Lambda}$ and $\boldsymbol{\xi}^{(0)} \in \Theta_{\Pi}$, there exists $\rho^* > 0$ for which the optimization problems (13) and (14) admit unique solutions for any $\rho \in (0, \rho^*]$.
- b. If ρ belongs to $(0, \rho^*]$, then the iterative spitting-projection numerical scheme stated in Algorithm 3.3 converges to a unique solution.

Remark 3.5. Note that the solution of Problem (10) can be obtained by Algorithm 3.3 for appropriate choices of the individual regularization parameters ρ_{Λ} and ρ_{Π} .

3.4 Single profile registration to the mean shape

Next, we consider the registration problem of a profile f_j (not necessarily belonging to the training set \mathcal{F}) to the mean profile f_0 . This can also be realised as the best approximation problem of a f_j through the SIM deformation of f_0 (as estimated through the procedure presented in Section 3.3). This leads to the profile registration problem

$$(15) \quad \min_{\theta \in \Theta_R} V_j(\theta) = \min_{\theta \in \Theta_R} \langle f_j - \hat{f}(\theta), f_j - \hat{f}(\theta) \rangle$$

where $\hat{f}(\theta) = \beta + \alpha f_0(\kappa^{-1}(t - \zeta))$ and

$$(16) \quad \Theta_R := \left\{ \theta = (\alpha, \beta, \kappa, \zeta)' : \begin{array}{l} \alpha \in (0, \alpha_{\max}], \quad \beta \in [\beta_{\min}, \beta_{\max}], \\ \kappa \in (0, \kappa_{\max}], \quad \zeta \in [\zeta_{\min}, \zeta_{\max}] \end{array} \right\}$$

with the lower and upper bounds of the parameters are subject to the characteristics of the profiles f_0 and f_j . Problem (15) although admits solutions by standard continuity arguments, it is not necessary for the solution to be unique. This problem practically concerns only the phase deformation parameters (κ, ζ) , since the same problem is strictly convex (quadratic) with respect to the amplitude deformation parameters (α, β) . Therefore, a regularization term is needed for the successful treatment of the problem which will importantly play the role of a selection criterion when more than one minimizers exist. In that case, we would like to chose that θ which causes the smallest possible deformation to the reference shape f_0 in order to represent f_j . In the same spirit with Section 3.3, we consider quadratic regularization terms concerning the aggregate deformation effect, caused by the choice of an arbitrary $\theta = (\alpha, \beta, \kappa, \zeta)'$, stating our preference to the minimum possible deformation. Then, it can be shown that for a certain value of the sensitivity parameter ρ and below, the single profile registration problem admits unique solution. However, note that the introduced regularization term is not necessary to involve all the parameters in θ , but only κ, ζ , since closed-form solutions for α, β can be attained given κ, ζ (please see the relevant discussion in the Appendix A.3).

Proposition 3.6. *Let $f_0 \in L^2(I)$ be a reference shape and $f_j \in L^2(I)$ a profile to be registered to it as a SIM deformation. There exists $\rho_* > 0$ for which the single profile registration problem*

$$(17) \quad \min_{\theta \in \Theta_R} \left\{ V_j(\theta) + \frac{1}{2\rho} \|\theta\|_2^2 \right\}$$

where V_j determined in (15), admits unique solution for any $\rho \in (0, \rho_*]$.

For the proof please see Appendix A.3.

4 The Exponentially Weighted Fréchet Moving Average scheme for functional profiles

Following the characterization and estimation of the typical profile in Section 3, the construction of an EWMA-type procedure for detecting potential shifts with respect to the underlying shape and deformations from it, is proposed. Our interest focuses on the case of curves representing the evolution of a quantity in a specified time (or space) interval $t \in I$, whose pattern can be efficiently calibrated by the shape invariant model as discussed above. The rationale behind the developed control chart, is similar to the classical EWMA charts procedure either for monitoring the mean or variability process of the statistical quantities under study (see e.g. Montgomery (2009)).

The novelty of the proposed shift detection scheme relies on the fact that a generalized mean sense is incorporated directly in the chart element estimation procedure, providing an attractive framework for analyzing functional data parameterizing certain characteristics of them. In what follows, a modification of the EWMA monitoring approach is presented, in which, the mean sense derived by the notion of the Fréchet mean is deployed for the development of an exponentially weighted scheme, able to be implemented directly to the metric space of the profiles under study. This modification enables the development of the first branch of the proposed shift detection scheme, which allows for the monitoring of significant changes to the underlying shape of the profile under study. At the second step, a Fréchet mean based scheme is built for the surveillance of the shape deformation processe (according to the shape invariant model) which quantify the deviations of the profile under study from the reference pattern. The aforementioned steps provide a two-stage shift detection framework capable of explaining potential shifts of the profile under study and interpret them either as *shape shifts* (i.e. significant shift to the underlying shape) or *deformation shifts* (i.e. significant shifts to the aggregate deformation effect with respect to the reference shape). In the sequel, we use the term Exponentially Weighted Fréchet Moving Average (EWFMA) when refer to the proposed scheme.

4.1 Shift detections on the underlying shape

Given a training set of n in control (IC) profiles $\mathcal{F} = \{f_1, \dots, f_n\}$, the typical profile f_0 is estimated through the procedure described in Section 3, under the assumption that any IC element is acceptably deviant from the mean shape f_0 with respect to the shape invariant model. Being acceptably deviant means both that (a) the underlying shape of the profile and (b) the respective amplitude-phase deformation process (as captured by the shape invariant model), produce aggregate deviance levels that do not exceed the ones observed from the IC dataset \mathcal{F} . Given the estimated IC behaviour f_0 , for a newly sampled f_j , the best approximation according to model (3) is obtained through the solution of the related registration problem stated in (17).

At the first stage of the EWFMA scheme, a chart for monitoring the shape deviance process is constructed, i.e. the deviance of the underlying shape for a profile f_j (after removing the amplitude and phase deformation characteristics as estimated from (17)) from the reference

one. The retrieved underlying shape for the j -th profile given the obtained optimal deformation parameters θ_j , is defined as

$$(18) \quad \hat{f}_{0,j} = \alpha_j^{-1} (f_j(\kappa_j t + \zeta_j) - \beta_j).$$

Then, the underlying shape deviance between the j -th individual's underlying shape and the typical shape f_0 is calculated as

$$(19) \quad D_j^s := d_M^2(\hat{f}_{0,j}, f_0)$$

where d_M denotes the metric sense under which the deviance is determined (L^2 -distance in this paper). If the underlying shape for a profile is dramatically divergent from the typical one, then the shape invariant model is incapable of modelling the current observation and therefore the examined profile should be considered as an OOC one (i.e. not explainable from the current deformation model). As a result, the following EWMA-type scheme for monitoring the underlying shape deviance process is proposed:

$$(20) \quad \begin{cases} \tilde{D}_j^s = \lambda D_j^s + (1 - \lambda) \tilde{D}_{j-1}^s, & \lambda \in (0, 1], \quad j = 1, 2, \dots \\ \tilde{D}_0^s = 0 \end{cases}$$

The bounds beyond which the deviance process provides a shift, can be estimated by the empirical distribution of shape deviances from the IC profiles given certain confidence levels.

4.2 Shift detections on the deformation characteristics

Assuming that no shift in the underlying shape is detected, the profile under study can be described by the shape invariant model, while at the next step, its deformation characteristics (amplitude and phase deformations) are examined. For this task, a separate exponentially weighted chart is developed, relying on the formulation of the shape invariant model combined with the notion of the Fréchet mean. The resulting chart concerns the deformations deviance process, i.e. the total deformation effect performed by both amplitude and phase deformations to the underlying shape. In this view, each profile (since it has been already considered as in control in terms of preserving the typical shape f_0) is identified by its modelling counterpart, i.e. $\hat{f}_j = \hat{f}(\theta_j)$ where θ_j is the minimizer of the related registration problem stated in (17) and $\hat{f}(\theta)$ representing the fitted part of f_j from (3) (without the error term). This second stage of the EWMA scheme is built directly on the modelled profiles with respect to the Fréchet mean sense. Initializing the monitoring procedure with the reference profile f_0 , each new element of the scheme is naturally derived as the Fréchet mean of the profiles f_0 and \hat{f}_j with corresponding weights λ and $1 - \lambda$, leading to the variational problem

$$(21) \quad \tilde{f}_j := \arg \min_{g \in \mathcal{M}} \left\{ \lambda d_M^2(g, \hat{f}_j) + (1 - \lambda) d_M^2(g, \tilde{f}_{j-1}) \right\}, \quad \tilde{f}_0 = f_0.$$

Since we are interested in the deformation characteristics with respect to f_0 , we consider a reduced version of the variational problem stated above, by substituting $g = \hat{f}(\theta)$ resulting to the simpler fitting problem

$$(22) \quad \min_{\theta \in \Theta_R} V_\lambda(\theta) = \min_{\theta \in \Theta_R} \left\{ \lambda \|\hat{f}(\theta) - \hat{f}_j\|_2^2 + (1 - \lambda) \|\hat{f}(\theta) - \tilde{f}_{j-1}\|_2^2 \right\}, \quad \lambda \in (0, 1]$$

where Θ_R is the set defined in (16). For the same reasons discussed in Section 3.4, the above problem does not necessarily admit unique solution, and a regularized version of the problem similar to the one in Proposition 3.6 is considered. In a similar manner, the regularization term turns the problem to a strictly convex one with respect to θ and at the same time introduces

a selection criterion when multiple minima occur. The related result follows (for details on the proof please see Appendix B.1).

Proposition 4.1. *Let $f_0 \in L^2(I)$ be the mean pattern and $\hat{f}, \tilde{f} \in L^2(I)$ be two reference profiles. There exists $\tilde{\rho}_* > 0$ for which the chart element estimation problem*

$$(23) \quad \min_{\theta \in \tilde{\Theta}} \left\{ V_\lambda(\theta) + \frac{1}{2\rho} \|\theta\|_2^2 \right\}$$

where V_λ determined in (22), admits unique solution for any $\rho \in (0, \tilde{\rho}_*]$.

Following the above result, in the general setting the EWFMA chart elements are obtained through the scheme

$$(24) \quad \begin{cases} \tilde{\theta}_j = \arg \min_{\theta \in \tilde{\Theta}} \left\{ \lambda \|\hat{f}(\theta) - \hat{f}_j\|_2^2 + (1 - \lambda) \|\hat{f}(\theta) - \tilde{f}_{j-1}\|_2^2 + R_\rho(\theta) \right\}, \\ \tilde{\theta}_0 = (\tilde{\alpha}_0, \tilde{\beta}_0, \tilde{\kappa}_0, \tilde{\zeta}_0)' = (1, 0, 1, 0)' \end{cases}$$

Determining the optimal parameters $\tilde{\theta}_j$ is equivalent to the determination of \tilde{f}_j in problem (21) under the shape invariant model framework. Then, the modelled profiles chart elements are obtained in a compatible to the space \mathcal{M} sense, through the notion of the Fréchet mean. The relevant chart for monitoring the modelled profiles deviance process (or simply the deformations deviance process) is constructed as

$$(25) \quad \begin{cases} \tilde{D}_j^\theta = \lambda D_j^\theta + (1 - \lambda) \tilde{D}_{j-1}^\theta, & \lambda \in (0, 1], \quad j = 1, 2, \dots \\ \tilde{D}_0^\theta = 0 \end{cases}$$

where $D_j^\theta := \|\hat{f}(\theta_j) - f_0\|_2^2$ with control limits of the chart to be specified by the induced empirical distribution from the training set.

Remark 4.2. One may consider beginning the shift detection procedure by building typical EWMA charts on the obtained deformation parameters and then extending this chart for the deformation processes and the object f_j , as well. However, non-linearity of f_j with respect to the parameters (in particular for the shape invariant model with respect to the phase deformation parameters) does not allow for such a generalization. Notice that assuming that the deformation functions Λ, Π are linear with respect to their parameters, e.g. $\Lambda(z) = \beta + \alpha z$, $\Pi(s) = \zeta + \kappa s$, although one may attempt to monitor the deformation functions separately, e.g. $\tilde{\Lambda}_j = \lambda \Lambda_j + (1 - \lambda) \tilde{\Lambda}_{j-1}$ and $\tilde{\Pi}_j = \lambda \Pi_j + (1 - \lambda) \tilde{\Pi}_{j-1}$, then the resulting chart for f_j through $\tilde{f}_j = \lambda \tilde{\Lambda}_j \circ f_0 \circ \tilde{\Pi}_j + (1 - \lambda) \tilde{f}_{j-1}$ does not coincide with the minimizer of equation (21).

4.3 The functional profiles shift detection algorithm

Combining the two shift detection schemes described in (20) and (25) results to an effective tool for both detecting and explaining potential shifts for profiles which can be captured by the parameterization offered by the shape invariant model. At the first step, we check if the observed profile's underlying shape is sufficiently close to the estimated typical pattern (f_0). If a shift is detected at this step, then the profile is considered as an out of control (OOC) one, at least under the shape invariant model's explainability. If no shift detected, then the shape invariant model can be considered as a valid approach and we proceed with studying its amplitude-phase deformation characteristics. At this step, the second monitoring approach is applied and determines whether the aggregate deformation effect leads to an IC status for the examined profile or not. If no shift is detected, the profile is considered as an IC one, while in the opposite case, we further investigate which deformation attributes led to the shift by constructing typical EWMA charts on each one of the deformation parameter in θ_j . A

graphical representation of the monitoring procedure is illustrated in Figure 2 while the steps of the monitoring scheme are briefly described in Algorithm 4.3.

Algorithm 4.3 (The EWFMA shifts detection scheme).

- **Phase I: Mean profile and IC profiles characteristics determination**

(a) *Mean pattern estimation*

Given a set of IC profiles $\mathcal{F} = \{f_1, f_2, \dots, f_n\}$ estimate the mean profile f_0 according to the procedure described in Section 3.2.

(b) *Estimation of the IC profiles deformation characteristics*

Determine the deformation characteristics of all IC profiles with respect to f_0 following the procedure described in Section 3.4

- **Phase II: Detection of shape and/or deformation shifts**

(a) *Shift detection on the underlying shape*

Given $\lambda > 0$, for a newly sampled profile f_j apply the procedure described in (20) and determine if the underlying shape of the profile f_j is significantly shifted w.r.t. the reference mean shape f_0 . If no shift is detected, proceed to Step II(b).

(b) *Shift detection on the deformation process*

Apply the chart described in (25) to determine if the aggregate amplitude-phase deformation is an IC one. If shift detected, check individual deformation characteristics (deformation parameters) through individual EWMA charts for the parameters obtained by (24).

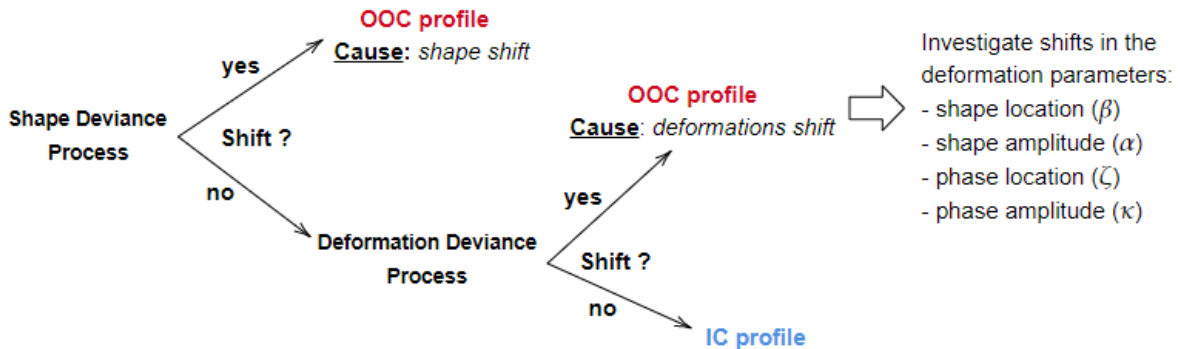


Figure 2: Graphical illustration of the presented scheme profile monitoring process.

4.4 Analysis of ambient air quality profiles in the area of Athens

In this section, the presented methodology is implemented to the analysis of air pollution profiles in an area of the city of Athens. The discussed approach has been also priorly tested with success to a number of simulation experiments with synthetic types of data. Since, all the important aspects and capabilities of the method that have been displayed in the synthetic data experiments are fully observed through the air pollution case study without losing any part of the stress assessment of the approach, and taken into account: (a) the better insights provided by a real world example and (b) having in mind to keep the paper coinsize, we illustrate only the real world example. The functional modelling and shift detection approach presented in Section 3 is employed in studying daily air pollution data that have been recorder by atmospheric pollution sensors from the area of Patission Street in Athens, installed by the Ministry of Environment and Energy.

The study concerns the task of monitoring ambient air quality in this area for the time period 2001-2007 under the functional data setting. The available data³ consist of hourly measurements (mean values per hour for the duration of a day, i.e. 24 measurements) of the concentration of four chemical quantities considered as potential pollutants, and specifically, the concentration of: carbon monoxide (CO), nitrogen dioxide (NO₂), ozone (O₃) and sulfur dioxide (SO₂). Certain safety concentration thresholds for the human health concerning the pollutants concentration in the regional atmosphere have been set by the recent directions of the World Health Organization⁴ (WHO) (please see Table 1). According to these guidelines, a day in which at least one of the thresholds has been violated is characterized as an OOC day, while if none has been violated is considered as an IC day. This classification strategy is adopted in the experiment for distinguishing between IC and OOC profiles. However, note that these thresholds are constantly been revised by WHO with the tendency to become more strict through the years.

Pollutant	Time Interval	Unit	Maximum Average Concentration Threshold
Carbon Monoxide (CO)	1 hr	mg/m ³	≤ 35
	8 hrs	mg/m ³	≤ 10
	24 hrs	mg/m ³	≤ 4
Nitrogen Dioxide (NO ₂)	1 hr	μg/m ³	≤ 200
	24 hrs	μg/m ³	≤ 25
Ozone (O ₃)	8 hrs	μg/m ³	≤ 60
Sulfur Dioxide (SO ₂)	24 hrs	μg/m ³	≤ 40

Table 1: Safety concentration thresholds of the pollutants under study for human health according to the World Health Organization

This threshold-based approach is maybe not the best strategy for the efficient and successful monitoring of ambient air quality, since the actual nature of data is of functional form while the threshold is defined pointwise (with respect to time and space). Under this perspective, it could be possible a pollutant’s concentration to be in quite high levels during all the day but never exceeding the nominal threshold value. Therefore such a profile, although not considered as an OOC one, it would provide significant risks for the public health. The discussed functional approach provides an alternative tool for assessing and measuring the status of such phenomena that evolve simultaneously with similar manner (with small fluctuations around a specific standard). Employing the framework of deformation models in the profile modelling task, and in particular exploiting the explanatory capabilities of the shape invariant model, allows for the recovery and quantification of special characteristics that cannot be captured by typical pointwise approaches. To illustrate the capabilities of the discussed method, we use as training dataset the recorded profiles from the time period 2001-2004, and as test dataset the records from the time period 2005-2007. Note that we focus on the months October, November and December in our analysis, since it is considered as the "peak period" for the concentration of pollutants in the atmosphere (i.e. it is more interesting in terms of identifying the OOC days). Moreover, in these three months no significant differences in the environmental conditions are observed and the median levels of the polluters are quite the same (similar median estimated curves) and as a result, seasonality effect is not an issue.

During the phase I of the monitoring procedure, the IC observations from the time period 2001-2004 are used as the trainset and the typical behaviour for the intra-day concentration of each pollutant (i.e. the typical curve representing the daily evolution of each pollutant) alongside with the respective deformations around the mean patterns and their induced em-

³Data are publicly available at:
<https://ypen.gov.gr/perivallon/poiotita-tis-atmosfairas/dedomena-metriseon-atmosfairikis-rypansis/>
⁴[https://www.who.int/news-room/fact-sheets/detail/ambient-\(outdoor\)-air-quality-and-health](https://www.who.int/news-room/fact-sheets/detail/ambient-(outdoor)-air-quality-and-health)

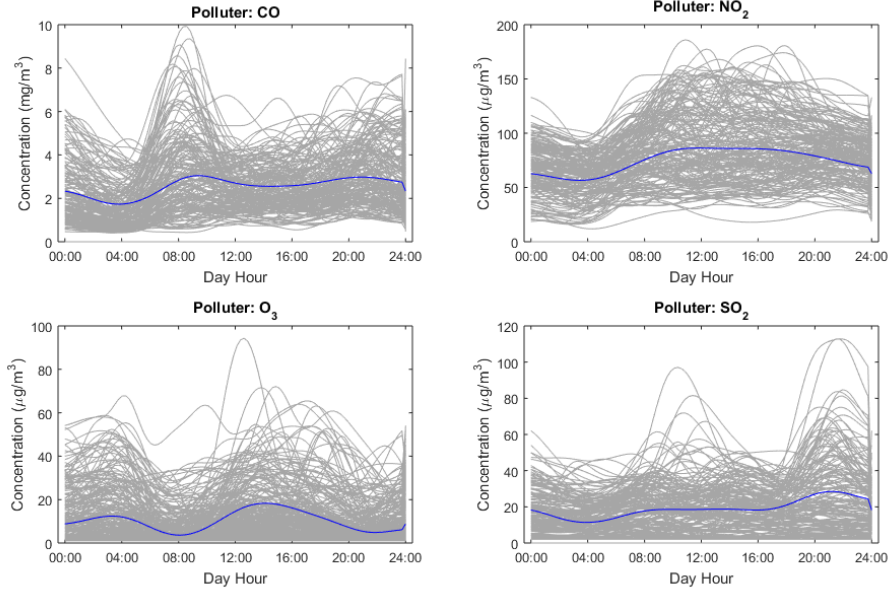


Figure 3: The calculated typical profiles (blue lines) for the intra-day (per hour) concentration of each one of the pollutants (CO, NO₂, O₃, SO₂) in the regional atmosphere.

pirical distributions are estimated. A slightly modified version of the shape invariant model is incorporated where the phase scaling parameter κ is omitted to simplify the analysis. The deformation characteristics parameterized by the SIM (location, amplitude and phase) allow for a more careful and meaningful representation of the potential deviations from the reference pattern that could possibly affect the pollutant's status at each day. Each one of the considered pollutants display quite different concentration behaviour which enables the assessment of the presented methodology under different conditions and data patterns. In Figure 3 are illustrated the IC daily concentration curves of the pollutants under study (recorded in the training set) and their estimated mean patterns (typical concentration profiles). All data patterns seems to be successfully calibrated by the shape invariant model and the calculated Fréchet means, representing plausibly the typical behaviours of the pollutants' concentration in the city's regional atmosphere.

Subsequently, the phase II of the functional monitoring scheme is performed and the method is assessed over the test dataset concerning the time period 2005-2007. Following the described procedure, the EWFMA control charts for the sampled profiles are constructed to detect significant shifts either in shape and/or in the deformation process. The resulting diagnostic charts are depicted for each pollutant under study in Figures 4, 5, 6 and 7. In the upper panel, the deviance related charts are displayed with respect to the reference shape (left column) and the total deformation effect with respect to the estimated mean pattern (right column). The second panel of charts concerns shifts with respect to the individual deformation features explained by the shape-invariant model (shape location, shape amplitude and phase shift). Note that the Fréchet mean is calculated according to the L^2 -metric sense, while exponential weighting parameters on the grid

$$\lambda = 0.01, 0.02, \dots, 0.05, 0.10, \dots, 0.90, 0.95, 0.96, \dots, 0.99$$

have been tested. The optimal choice was selected per case (by optimality we mean to seek the value of λ for which less OOC observations are classified as IC and less IC observations are classified as OOC, i.e. minimizing both type-I and type-II errors). Although, one could try to occasionally reallocate the weighting parameter value by separating the train set to further

parts and re-arranging the values according to cross-validation findings, we feel that such a task is beyond the scopes of this work and therefore we use a constant value for each pollutant for the whole monitoring task.

Pollutant	Monitoring Process	Number of Cases	Classification Accuracy		Per Class Accuracy	
			True (%)	False (%)	OOC (%)	IC (%)
CO	both	266	87.22 (232)	12.78 (34)	100.00 (71)	82.56 (161)
	shape process	266	69.55 (185)	30.45 (81)	2.82 (2)	93.85 (183)
	deformation process	266	91.35 (243)	8.65 (23)	100.00 (71)	88.21 (172)
NO ₂	both	264	82.58 (218)	17.42 (46)	78.26 (18)	82.99 (200)
	shape process	264	81.82 (216)	18.18 (48)	0.00 (0)	89.63 (216)
	deformation process	264	84.85 (224)	15.15 (40)	78.26 (18)	85.48 (206)
O ₃	both	266	88.35 (235)	11.65 (31)	100.00 (1)	88.30 (234)
	shape process	266	96.99 (258)	3.01 (8)	0.00 (0)	97.36 (258)
	deformation process	266	90.23 (240)	9.77 (26)	100.00 (1)	90.19 (239)
SO ₂	both	266	95.86 (255)	4.14 (11)	100.00 (55)	94.79 (200)
	shape process	266	77.44 (206)	22.56 (60)	0.00 (0)	97.63 (206)
	deformation process	266	96.62 (257)	3.38 (9)	100.00 (55)	95.73 (202)

Table 2: Per stage performance of the functional EWMA-type monitoring scheme for each pollutant

In Table 2 are illustrated the performance diagnostics for each monitoring stage of the method concerning: (a) the shape process, (b) the deformation process and (c) the profile in total, relying on the modelling capabilities and explainability of the shape invariant model. The shift detection scheme displayed in general a nice performance in identifying the shifts (according to the threshold definition of WHO discussed above) with true classification percentages between 82–96%. Clearly, the pollutants CO and NO₂ can be characterized as the more difficult cases where higher error rates are observed, while the SO₂ is the pollutant where the scheme displayed the best accuracy. From the results, concerning the underlying shape process monitoring (rows about the shape process in Table 2 and the first deviance plot in the upper panel of the individual figures per pollutant) it is evident that the SIM is appropriate for describing such type of profiles, since too few cases are indicated as not explainable by this model (OOC cases). Note that in the table the results have been calculated according to the classification by WHO and not according to actual shape shifts identifications. The deformation process shift detection scheme performed also decently in identifying actual shifts for the pollutants CO, O₃ and SO₂ with total true classification percentage between 90–96% and zero probabilities in conducting type-I error. However, in the case of NO₂ the error rates are much higher (around 15–20%). The individual deformation characteristics can be further investigated through the individual deformation parameter charts when a shift is detected. For all pollutants, the phase shift attribute quantified by the parameter ζ seems not to be related to the actual shifts and in the majority of cases, the related charts do not display behaviours beyond the limits. On the contrary, the phase amplitude parameter α and in some cases the vertical shift parameter β identify the significant changes (shape deformations) in the daily concentration profiles as displayed from the relevant plots (see second panel of graphs in Figures 4, 5, 6 and 7). In general, it seems that amplitude deformation level can be used as a proxy for detecting significant shifts when shape process is in control.

5 Conclusions

In this work a framework for the statistical monitoring of functional data by combining the notion of the Fréchet mean and the framework of the shape invariant deformation model is proposed and is implemented to the important environmental problem of air quality monitoring. The well known shape invariant model has been studied as a modeling approach of the respective functional profiles representing each one as a distortion of the typical pattern that should

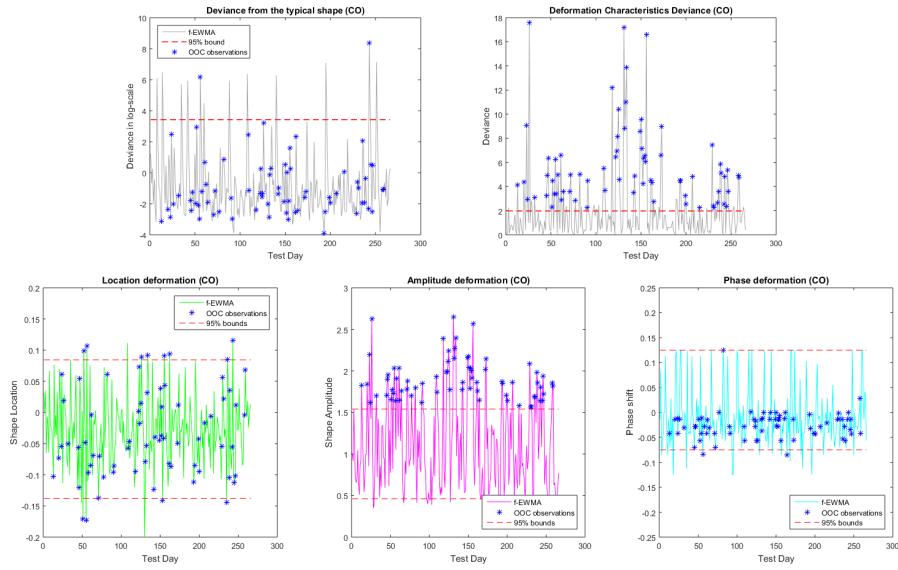


Figure 4: The EWFMA control charts for monitoring shape and deformations deviances (upper panel) and for the individual deformation characteristics (lower panel) for CO.

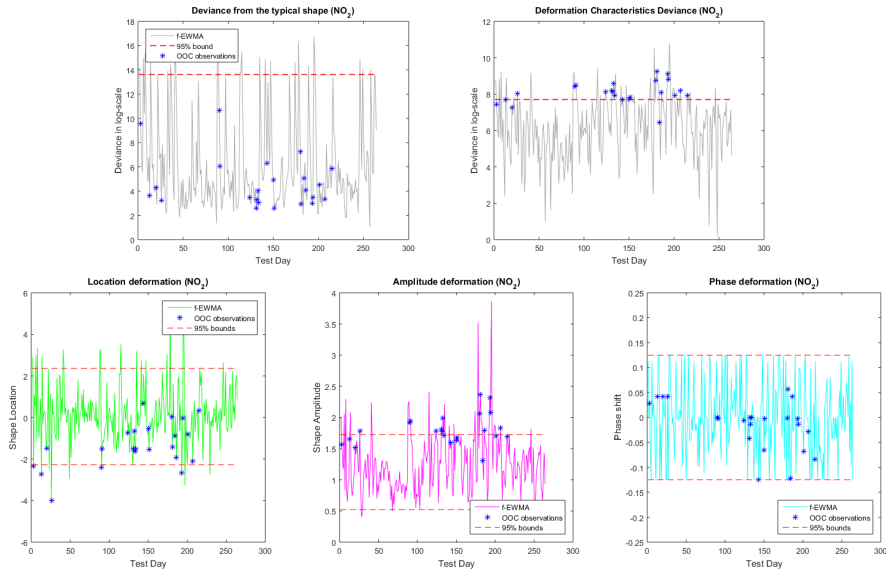


Figure 5: The EWFMA control charts for monitoring shape and deformations deviances (upper panel) and for the individual deformation characteristics (lower panel) for NO₂.

be observed, i.e. the Fréchet mean of a training set of profiles. The combination of these frameworks offers the following advantages: (a) a computationally effective way to estimate the Fréchet mean since the computational cost is significantly reduced by transforming the related optimization problem from a variational one to a fitting one, and (b) the deformation modelling approach which allows for the classification of potential shifts of the profiles either to shifts in the underlying shape and/or to shifts in certain characteristics of the deformation process. The relevant functional monitoring scheme has been applied with success in a real-world example where air pollution profiles in the city of Athens were studied and shape shifts are successfully identified in most of the cases.

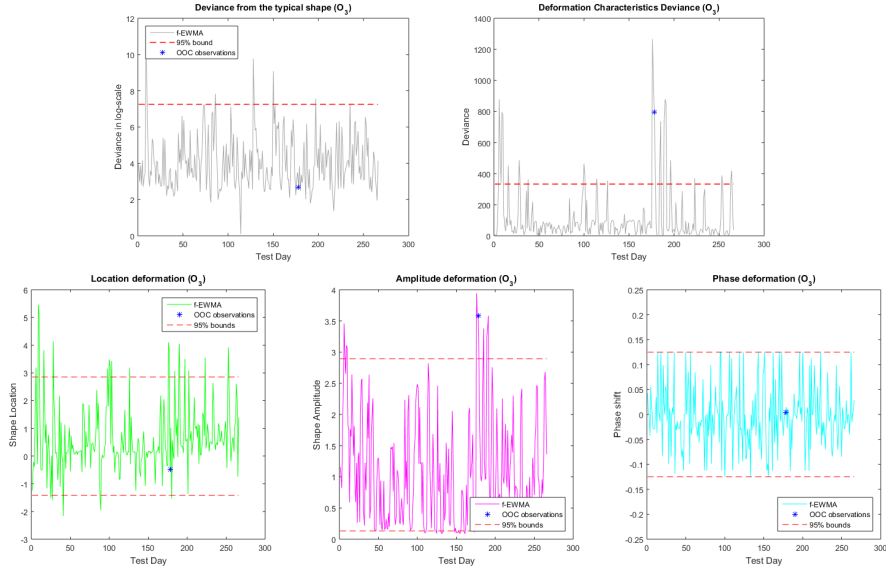


Figure 6: The EWFMA control charts for monitoring shape and deformations deviances (upper panel) and for the individual deformation characteristics (lower panel) for O_3

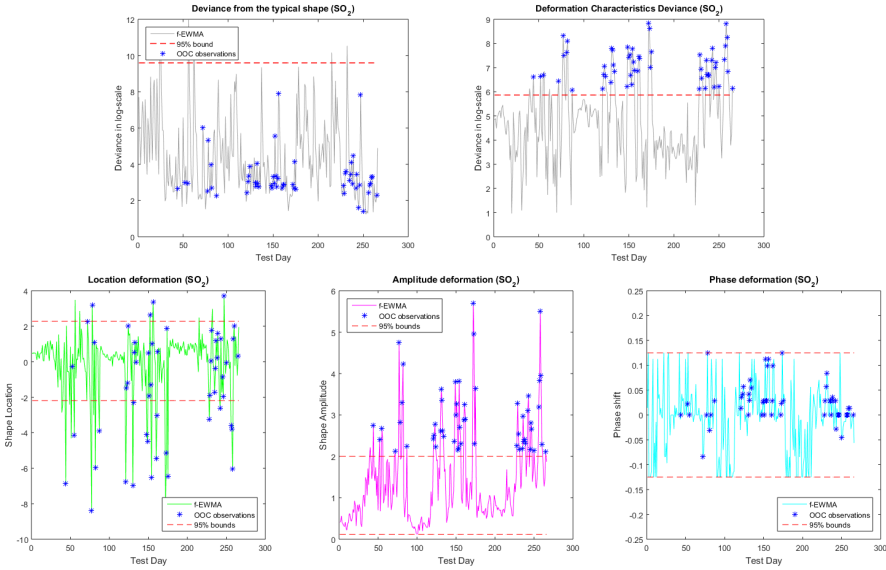


Figure 7: The EWFMA control charts for monitoring shape and deformations deviances (upper panel) and for the individual deformation characteristics (lower panel) for SO_2

Funding

Two of the authors wish to acknowledge for financial support from the research program DRASI II, funded by the AUEB Research Center.

References

- Afsari, B. (2011). Riemannian l^p center of mass: existence, uniqueness and convexity. *Proceedings of the American Mathematical Society* 139(2), 655–673.
- Arnaudon, M., F. Barbaresco, and L. Yang (2013). Medians and means in Riemannian geome-

- try: existence, uniqueness and computation. In *Matrix Information Geometry*, pp. 169–197. Springer.
- Bauschke, H. H. and J. M. Borwein (1993). On the convergence of von Neumann’s alternating projection algorithm for two sets. *Set-Valued Analysis* 1(2), 185–212.
- Bauschke, H. H. and J. M. Borwein (1994). Dykstra’s alternating projection algorithm for two sets. *Journal of Approximation Theory* 79(3), 418–443.
- Beath, K. J. (2007). Infant growth modelling using a shape invariant model with random effects. *Statistics in medicine* 26(12), 2547–2564.
- Bigot, J., B. Charlier, et al. (2011). On the consistency of Fréchet means in deformable models for curve and image analysis. *Electronic Journal of Statistics* 5, 1054–1089.
- Bigot, J., S. Gadat, and J.-M. Loubes (2009). Statistical M-estimation and consistency in large deformable models for image warping. *Journal of Mathematical Imaging and Vision* 34(3), 270–290.
- Bigot, J., X. Gendre, et al. (2013). Minimax properties of Fréchet means of discretely sampled curves. *The Annals of Statistics* 41(2), 923–956.
- Cano, J., J. M. Moguerza, S. Psarakis, and A. N. Yannacopoulos (2015). Using statistical shape theory for the monitoring of nonlinear profiles. *Applied stochastic models in business and industry* 31(2), 160–177.
- Centofanti, F., A. Lepore, A. Menafoglio, B. Palumbo, and S. Vantini (2021). Functional regression control chart. *Technometrics* 63(3), 281–294.
- Chicken, E., J. J. Pignatiello Jr, and J. R. Simpson (2009). Statistical process monitoring of nonlinear profiles using wavelets. *Journal of Quality Technology* 41(2), 198–212.
- Dryden, I. L. and K. V. Mardia (2016). *Statistical shape analysis: with applications in R*, Volume 995. John Wiley & Sons.
- Dubey, P. and H.-G. Müller (2019). Fréchet analysis of variance for random objects. *Biometrika* 106(4), 803–821.
- Fassò, A., M. Toccu, and M. Magno (2016). Functional control charts and health monitoring of steam sterilizers. *Quality and Reliability Engineering International* 32(6), 2081–2091.
- Fréchet, M. (1948). Les éléments aléatoires de nature quelconque dans un espace distancié. In *Annales de l’institut Henri Poincaré*, Volume 10, pp. 215–310.
- Gervini, D. and T. Gasser (2004). Self-modelling warping functions. *Journal of the Royal Statistical Society: Series B (Statistical Methodology)* 66(4), 959–971.
- Harris, T., J. D. Tucker, B. Li, and L. Shand (2020). Elastic depths for detecting shape anomalies in functional data. *Technometrics*, 1–11.
- Izem, R., J. S. Marron, et al. (2007). Analysis of nonlinear modes of variation for functional data. *Electronic Journal of Statistics* 1, 641–676.
- Jung, S., I. L. Dryden, and J. Marron (2012). Analysis of principal nested spheres. *Biometrika* 99(3), 551–568.
- Kampelis, N., I. G. Papayiannis, et al. (2020). An integrated energy simulation model for buildings. *Energies*.

- Kneip, A. and J. Engel (1995). Model estimation in nonlinear regression under shape invariance. *The Annals of Statistics*, 551–570.
- Kravvaritis, D. C. and A. N. Yannacopoulos (2020). *Variational Methods in Nonlinear Analysis: With Applications in Optimization and Partial Differential Equations*. Walter de Gruyter GmbH & Co KG.
- Le, H. and A. Kume (2000). The fréchet mean shape and the shape of the means. *Advances in Applied Probability*, 101–113.
- McGinnity, K., E. Chicken, and J. J. Pignatiello Jr (2015). Nonparametric changepoint estimation for sequential nonlinear profile monitoring. *Quality and Reliability Engineering International* 31(1), 57–73.
- Moguerza, J. M., A. Muñoz, and S. Psarakis (2007). Monitoring nonlinear profiles using support vector machines. In *Iberoamerican congress on pattern recognition*, pp. 574–583. Springer.
- Montgomery, D. C. (2009). *Statistical quality control*, Volume 7. Wiley New York.
- Panaretos, V. M., Y. Zemel, et al. (2016). Amplitude and phase variation of point processes. *The Annals of Statistics* 44(2), 771–812.
- Papayiannis, G. I., E. A. Giakoumakis, et al. (2018). A functional supervised learning approach to the study of blood pressure data. *Statistics in medicine* 37(8), 1359–1375.
- Paynabar, K., C. Zou, and P. Qiu (2016). A change-point approach for phase-I analysis in multivariate profile monitoring and diagnosis. *Technometrics* 58(2), 191–204.
- Petersen, A., H.-G. Müller, et al. (2019). Fréchet regression for random objects with euclidean predictors. *The Annals of Statistics* 47(2), 691–719.
- Qiu, P., C. Zou, and Z. Wang (2010). Nonparametric profile monitoring by mixed effects modeling. *Technometrics* 52(3), 265–277.
- Shiau, J.-J. H., H.-L. Huang, S.-H. Lin, and M.-Y. Tsai (2009). Monitoring nonlinear profiles with random effects by nonparametric regression. *Communications in Statistics: Theory and Methods* 38(10), 1664–1679.
- Small, C. G. (2012). *The statistical theory of shape*. Springer Science & Business Media.
- Wang, K., T. Gasser, et al. (1997). Alignment of curves by dynamic time warping. *The Annals of Statistics* 25(3), 1251–1276.
- Yu, G., C. Zou, and Z. Wang (2012). Outlier detection in functional observations with applications to profile monitoring. *Technometrics* 54(3), 308–318.
- Zemel, Y. and V. M. Panaretos (2019). Fréchet means and Procrustes analysis in Wasserstein space. *Bernoulli* 25(2), 932–976.
- Zhao, X. and E. Del Castillo (2021). An intrinsic geometrical approach for statistical process control of surface and manifold data. *Technometrics* 63(3), 295–312.

A Proof of Main Results in Section 3

A.1 Proof of Proposition 3.2

Proof of Proposition 3.2. Assume that f_0 and f_j for $j = 1, 2, \dots, n$ are sufficiently smooth functions. The objective function of the regularized problem, $J_\rho(\boldsymbol{\theta})$, is a continuous functions since both V and the regularization terms are continuous and hence, by standard arguments, it admits a solution in the compact set

$$\Theta := \left\{ \boldsymbol{\theta} = (\boldsymbol{\alpha}', \boldsymbol{\beta}', \boldsymbol{\kappa}', \boldsymbol{\zeta}')' \in \mathbb{R}^{4n} : \text{satisfying (8) and } \begin{array}{l} \alpha_j \in (0, \alpha_{\max}] \\ \beta_j \in [\beta_{\min}, \beta_{\max}] \\ \kappa_j \in (0, \kappa_{\max}] \\ \zeta_j \in [\zeta_{\min}, \zeta_{\max}] \end{array}, \forall j = 1, 2, \dots, n \right\}$$

where the lower and upper bounds are specified subject to the provided profiles f_0 and f_j for $j = 1, 2, \dots, n$. Moreover, note that the regularization term $R_\rho(\boldsymbol{\theta}) = \frac{1}{2\rho} \|\boldsymbol{\theta}\|_2^2$ for any $\rho > 0$ is a strictly convex function. By continuity arguments on the derivative of J_ρ for sufficiently small ρ , J_ρ remains strictly convex and hence admits a unique minimum. The critical value ρ_0 depends on the magnitude of the elements of the Hessian matrix of V . \square

A.2 Proof of Proposition 3.4

Proof of Proposition 3.4.

(a). Fixing $\boldsymbol{\xi}^{(0)} = \begin{pmatrix} \boldsymbol{\kappa}^{(0)} \\ \boldsymbol{\zeta}^{(0)} \end{pmatrix} \in \Theta_\Pi$, the regularized Fréchet function with respect to $\boldsymbol{\gamma} = \begin{pmatrix} \bar{\boldsymbol{\alpha}} \\ \bar{\boldsymbol{\beta}} \end{pmatrix}$ and for a certain choice $\rho > 0$ becomes

$$\begin{aligned} (26) \quad J_\rho(\boldsymbol{\gamma}) &:= V(\boldsymbol{\gamma}, \boldsymbol{\xi}^{(0)}) + \frac{1}{2\rho} (\|\bar{\boldsymbol{\alpha}}\|_2^2 + \|\bar{\boldsymbol{\beta}}\|_2^2 + \|\boldsymbol{\xi}^{(0)}\|_2^2) \\ &= \frac{1}{n} \bar{\boldsymbol{\alpha}}^T \tilde{C} \bar{\boldsymbol{\alpha}} + \frac{1}{n} \bar{\boldsymbol{\beta}} \mathbf{1} \mathbf{1}^T \bar{\boldsymbol{\beta}} + \mathbf{1}_n^T \hat{F} \\ &\quad - \frac{2}{n} \mathbf{1}_n^T \tilde{G} \bar{\boldsymbol{\alpha}} - \frac{2}{n} \mathbf{1}_n^T \bar{\boldsymbol{\beta}} F^T \mathbf{1}_n + \frac{2}{n} \mathbf{1}_n^T \bar{\boldsymbol{\beta}} \tilde{F}^T \bar{\boldsymbol{\alpha}} + \frac{1}{2\rho} (\bar{\boldsymbol{\alpha}}^T \bar{\boldsymbol{\alpha}} + \bar{\boldsymbol{\beta}}^T \bar{\boldsymbol{\beta}} + (\boldsymbol{\xi}^{(0)})^T \boldsymbol{\xi}^{(0)}) \end{aligned}$$

where $\tilde{f}_j(t) := f_j(\kappa_j^{(0)} t + \zeta_j^{(0)})$ for $j = 1, 2, \dots, n$ and

$$\begin{aligned} F &:= \begin{pmatrix} \int_I f_1(s) ds \\ \int_I f_2(s) ds \\ \vdots \\ \int_I f_n(s) ds \end{pmatrix} \in \mathbb{R}^n, \quad \tilde{F} := \begin{pmatrix} \int_I f_1(\kappa_1^{(0)} s + \zeta_1^{(0)}) ds \\ \int_I f_2(\kappa_2^{(0)} s + \zeta_2^{(0)}) ds \\ \vdots \\ \int_I f_n(\kappa_n^{(0)} s + \zeta_n^{(0)}) ds \end{pmatrix} \in \mathbb{R}^n, \quad \hat{F} := \begin{pmatrix} \langle f_1, f_1 \rangle \\ \langle f_2, f_2 \rangle \\ \vdots \\ \langle f_n, f_n \rangle \end{pmatrix} \in \mathbb{R}^n, \\ \tilde{C} &:= \begin{pmatrix} \langle \tilde{f}_1, \tilde{f}_1 \rangle & \langle \tilde{f}_1, \tilde{f}_2 \rangle & \dots & \langle \tilde{f}_1, \tilde{f}_n \rangle \\ \langle \tilde{f}_2, \tilde{f}_1 \rangle & \langle \tilde{f}_2, \tilde{f}_2 \rangle & \dots & \langle \tilde{f}_2, \tilde{f}_n \rangle \\ \vdots & \vdots & \ddots & \vdots \\ \langle \tilde{f}_n, \tilde{f}_1 \rangle & \langle \tilde{f}_n, \tilde{f}_2 \rangle & \dots & \langle \tilde{f}_n, \tilde{f}_n \rangle \end{pmatrix} \in \mathbb{R}^{n \times n}, \quad \tilde{G} := \begin{pmatrix} \langle f_1, \tilde{f}_1 \rangle & \langle f_1, \tilde{f}_2 \rangle & \dots & \langle f_1, \tilde{f}_n \rangle \\ \langle f_2, \tilde{f}_1 \rangle & \langle f_2, \tilde{f}_2 \rangle & \dots & \langle f_2, \tilde{f}_n \rangle \\ \vdots & \vdots & \ddots & \vdots \\ \langle f_n, \tilde{f}_1 \rangle & \langle f_n, \tilde{f}_2 \rangle & \dots & \langle f_n, \tilde{f}_n \rangle \end{pmatrix} \in \mathbb{R}^{n \times n}. \end{aligned}$$

Since function (26) is quadratic, taking first order conditions with respect to $\bar{\boldsymbol{\alpha}}$ and $\bar{\boldsymbol{\beta}}$ we obtain the linear system

$$(27) \quad \begin{pmatrix} \tilde{C} + \frac{1}{\rho} \mathbf{I} & \tilde{F} \mathbf{1}_n^T \\ \mathbf{1}_n \tilde{F}^T & \mathbf{1}_n \mathbf{1}_n^T + \frac{1}{\rho} \mathbf{I} \end{pmatrix} \begin{pmatrix} \bar{\boldsymbol{\alpha}} \\ \bar{\boldsymbol{\beta}} \end{pmatrix} = \begin{pmatrix} \tilde{G}^T \mathbf{1}_n \\ \mathbf{1}_n \mathbf{1}_n^T F \end{pmatrix}$$

where \mathbf{I} denotes the identity matrix in $\mathbb{R}^{n \times n}$. Then, there exists a maximum value ρ_Λ^* for which

the linear system (27) is explicitly solved for any $\rho \in (0, \rho_\Lambda^*]$ (since J_ρ becomes strictly convex).

Let us fix $\gamma^{(0)} = \begin{pmatrix} \bar{\alpha}^{(0)} \\ \bar{\beta}^{(0)} \end{pmatrix} \in \Theta_\Lambda$. The regularized Fréchet function with respect to ξ ,

$$J_\rho(\xi) := V(\gamma^{(0)}, \xi) + \frac{1}{2\rho}(\|\xi\|_2^2 + \|\gamma^{(0)}\|_2^2)$$

is a continuous function since both V and the regularization terms are continuous and hence, by standard arguments, it admits a solution in the compact set Θ_Π . Since, for any $\rho > 0$ the regularization term is a strictly convex function, by continuity arguments on the derivative of J_ρ for sufficiently small ρ , J_ρ remains strictly convex and hence admits a unique minimum. The critical value ρ_Π^* depends on the magnitude of the elements of the Hessian matrix of V .

Therefore, defining $\rho^* := \min(\rho_\Lambda^*, \rho_\Pi^*)$, then both problems (13) and (14) admit unique solutions for any ρ , strictly positive and at most equal to ρ^* . Moreover, since the projection operators $Proj_{\Theta_\Lambda}$ and $Proj_{\Theta_\Pi}$ are single-valued, the solution to the problems (13) and (14) are unique.

(b). Given that $\rho \in (0, \rho^*]$, uniqueness of solutions for the optimization problems (13) and (14) are guaranteed at each step of the algorithm by (a). At each iteration, the described numerical splitting scheme, generates a sequence of points $\{\theta_k\}_k$ by alternating projections between the two convex sets Θ_Λ and Θ_Π . In particular, at Step 1 the problem is solved on the convex set $\Gamma := \Theta \times \mathbb{R}^{2n}$ generating a sequence of points $\{\tilde{\theta}_k\}_k \subset \Gamma$, while at Step 2, the problem is solved on the convex set $\Xi := \mathbb{R}^{2n} \times \Theta_\Pi$ generating a sequence of points $\{\tilde{\theta}_k\}_k \subset \Xi$. It can be shown by the alternating projections algorithm (see e.g. Bauschke and Borwein (1993, 1994)) that as k grows, both sequences converge to a point θ_* in the intersection of the two sets $\mathcal{D} = \Gamma \cap \Xi$, being the minimizer of $J(\theta) := V(\theta) + \frac{1}{2\rho}\|\theta\|_2^2$. \square

A.3 Proof of Proposition 3.6 and auxiliary results

Proof of Proposition 3.6. The single profile regularized registration problem admits solutions since the objective function $J_\rho^{(j)}(\theta) := V_j(\theta) + \frac{1}{2\rho}\|\theta\|_2^2$ is a continuous function since both V and the regularization terms are continuous and hence, by standard arguments, it admits a solution in the compact set Θ_R as stated in (16). Due to strict convexity of the regularization term for any $\rho > 0$ and by continuity arguments on the derivative of $J_\rho^{(j)}$ for sufficiently small ρ , $J_\rho^{(j)}$ remains strictly convex and hence admits a unique minimum. The critical value ρ_* depends on the magnitude of the elements of the Hessian matrix of V_j . \square

Moreover, the solution can be parameterized since the amplitude deformation parameters (α, β) can be expressed in closed form as functions of the phase deformation parameters (κ, ζ) . The result is stated in the following Lemma.

Lemma A.1. *Given a pair of (κ, ζ) the optimal amplitude deformation parameters (α, β) of the single profile registration problem (15) admit the closed form*

$$(28) \quad \alpha_*(\kappa, \zeta) = \frac{\sigma_{0,j}(\kappa, \zeta)}{\sigma_0^2(\kappa, \zeta)}$$

$$(29) \quad \beta_*(\kappa, \zeta) = m_j - \alpha_*(\kappa, \zeta) m_0(\kappa, \zeta)$$

where $f_{0,\kappa,\zeta}(t) := f_0(\kappa^{-1}(t - \zeta))$ denotes the phase deformed mean profile and

$$\begin{aligned} m_0(\kappa, \zeta) &= \int_I f_{0,\kappa,\zeta}(t) dt, & m_j &:= \int_I f_j(t) dt \\ \sigma_0^2(\kappa, \zeta) &:= \langle f_{0,\kappa,\zeta}, f_{0,\kappa,\zeta} \rangle - m_0^2(\kappa, \zeta), & \sigma_{0,j}(\kappa, \zeta) &:= \langle f_{0,\kappa,\zeta}, f_j \rangle - m_0(\kappa, \zeta) m_j. \end{aligned}$$

the related moment terms.

Proof. The result is obtained by taking first order conditions to V_j as stated in (15) with respect to α, β and solving the resulting pair of equations. Continuity and strict convexity of V_j with respect to these parameters guarantee uniqueness for any pair (κ, ζ) . \square

B Proof of Main Result in Section 4

B.1 Proof of Proposition 4.1 and auxiliary results

Proof of Proposition 4.1. The chart element regularized estimation problem admits solutions since the objective function $\tilde{J}_\rho^{(j)}(\theta) := V_\lambda(\theta) + \frac{1}{2\rho}\|\theta\|_2^2$ is a continuous function since both V_λ and the regularization terms are continuous and hence, by standard arguments, it admits a solution in the compact set Θ_R as stated in (16). Due to strict convexity of the regularization term for any $\rho > 0$ and by continuity arguments on the derivative of $\tilde{J}_\rho^{(j)}$ for sufficiently small ρ , $\tilde{J}_\rho^{(j)}$ remains strictly convex and hence admits a unique minimum. The critical value $\tilde{\rho}_*$ depends on the magnitude of the elements of the Hessian matrix of V_λ . \square

In the same fashion with Proposition 3.6, the solution can be parameterized since the amplitude deformation parameters $(\tilde{\alpha}, \tilde{\beta})$ can be expressed in closed form as functions of the phase deformation parameters $(\tilde{\kappa}, \tilde{\zeta})$. The result is stated in the following Lemma.

Lemma B.1. *Given a pair of $(\tilde{\kappa}, \tilde{\zeta})$, the optimal amplitude deformation parameters $(\tilde{\alpha}, \tilde{\beta})$ for the chart element estimation problem described in (22) admit the closed form*

$$(30) \quad \tilde{\alpha}_\lambda(\tilde{\kappa}, \tilde{\zeta}) = \lambda \frac{\tilde{\sigma}_{0,j}(\tilde{\kappa}, \tilde{\zeta})}{\sigma_0^2(\tilde{\kappa}, \tilde{\zeta})} + (1 - \lambda) \frac{\tilde{\sigma}_{0,j-1}(\tilde{\kappa}, \tilde{\zeta})}{\sigma_0^2(\tilde{\kappa}, \tilde{\zeta})}$$

$$(31) \quad \tilde{\beta}_\lambda(\tilde{\kappa}, \tilde{\zeta}) = \lambda \hat{m}_j + (1 - \lambda) \tilde{m}_{j-1} - \tilde{\alpha}_\lambda(\tilde{\kappa}, \tilde{\zeta}) m_0(\tilde{\kappa}, \tilde{\zeta})$$

where $f_{0,\tilde{\kappa},\tilde{\zeta}}(t) := f_0(\tilde{\kappa}^{-1}(t - \tilde{\zeta}))$ denotes the phase deformed typical profile and

$$\begin{aligned} m_0(\tilde{\kappa}, \tilde{\zeta}) &= \int_I f_{0,\tilde{\kappa},\tilde{\zeta}}(t) dt, & \sigma_0^2(\tilde{\kappa}, \tilde{\zeta}) &:= \langle f_{0,\tilde{\kappa},\tilde{\zeta}}, f_{0,\tilde{\kappa},\tilde{\zeta}} \rangle - m_0^2(\tilde{\kappa}, \tilde{\zeta}) \\ \hat{m}_j &:= \int_I \hat{f}_j(t) dt, & \hat{\sigma}_{0,j}(\tilde{\kappa}, \tilde{\zeta}) &:= \langle f_{0,\tilde{\kappa},\tilde{\zeta}}, \hat{f}_j \rangle - m_0(\tilde{\kappa}, \tilde{\zeta}) \hat{m}_j \\ \tilde{m}_{j-1} &:= \int_I \tilde{f}_{j-1}(t) dt, & \tilde{\sigma}_{0,j-1}(\tilde{\kappa}, \tilde{\zeta}) &:= \langle f_{0,\tilde{\kappa},\tilde{\zeta}}, \tilde{f}_{j-1} \rangle - m_0(\tilde{\kappa}, \tilde{\zeta}) \tilde{m}_{j-1}. \end{aligned}$$

the related moment and variance terms.

Proof. The result is obtained by taking first order conditions to V_λ as stated in (22) with respect to $\tilde{\alpha}, \tilde{\beta}$ and solving the resulting pair of equations. Continuity and strict convexity of V_λ with respect to these parameters guarantee uniqueness for any pair $(\tilde{\kappa}, \tilde{\zeta})$. \square